Measurement and analysis of neutron spectra from thick targets of Al and Ti bombarded by 30–50 MeV α particles

D. Dhar and S. N. Roy
Department of Physics, Visva-Bharati, Santiniketan-731235, India

T. Bandyopadhyay and P. K. Sarkar
H.P. Unit, Variable Energy Cyclotron Centre, 1/AF, Bidhannagar, Calcutta-700064, India

(Received 19 June 2002; revised manuscript received 25 October 2002; published 24 February 2003)

Energy distributions of neutrons emitted from thick targets of ^{27}Al and ^{46}Ti are measured for alpha induced reactions at 30, 40, and 50 MeV projectile energies. Measurements are done at 0°, 30°, and 45° with respect to the projectile direction using the proton recoil scintillation technique. The measured data are compared with results from calculations using three different approaches of the exciton model namely, the master equation, the closed form and the hybrid model (a variant of the exciton model). The corresponding nuclear reaction model codes used for the purpose are PEQAG [E. Betak and J. Dobes, Report No. IP EPRC SAS 43/(1983), Bratislava, 1983], PRECO-D2, [C. Kalbach, Report No. LA-10248-MS, Los Alamos National Laboratory, Los Alamos, 1985] and ALICE91 [M. Blann, Lawrence Livermore National Laboratory Report No. UCID 19614, 1982], respectively. Proton induced neutron yield distributions measured by others are also included in the comparison. The calculated results from the hybrid model code ALICE91 give overall close approximations of the measured data compared to the other models.

DOI: 10.1103/PhysRevC.67.024607 PACS number(s): 24.10.−i, 25.55.−e, 29.30.Hs, 25.70.−z

I. INTRODUCTION

Measurement and analysis of thick target neutron yield (TTNY) distributions from nuclear reactions provide useful data for radiological safety and medical applications. Recently the development of spallation neutron sources have augmented interest in such data. Even though the emitted neutron spectrum from a thick target is a superposition of spectra from different stages of a continuously degrading projectile energy, analysis of such data gives insight into reaction mechanisms involved. Thickness of the target is so chosen that the projectile is completely stopped inside it. Thus in the case of thick targets, measurements at the extreme forward angle become possible. This helps understanding the reaction mechanism, particularly about the initial stages, since such information is mostly available with the emissions at forward angles.

We have measured neutron yield from thick targets of ^{46}Ti and ^{27}Al bombarded by 30–50 MeV α particles. These data have been analyzed in terms of three nuclear reaction model codes PEQAG [1] (master equation exciton model), PRECO-D2 [2] (closed form exciton model), and ALICE91 [3] (hybrid model) based on different formalisms. Predictive capabilities of these three nuclear reaction models are tested through comparisons with experimental observations. For the purpose of comparison we have also used the experimental data of [4] for 30 MeV proton induced neutron emission from thick targets of Fe, Cu, and Pb. Thick target neutron yield data from various target-projectile combinations have been analyzed by others in terms of Monte Carlo calculations of the intranuclear cascade (INC) and evaporation models [5]. These calculations are constrained by the lower limit set on the projectile energy. Nakamura and Uwamino [6] adopted a phenomenological hybrid model of preequilibrium and equilibrium emissions where both the spectra were fitted with two Maxwellian type functions having two different temperatures. However, neutron spectra calculated using this concept do not fit the experimentally observed data for light target nuclei, e.g., carbon. In an earlier work [7] the code PRECO-D2 was used to analyze TTNY distribution. It was found that the code underpredicted high energy component of emitted spectra. The necessities for theoretical estimation of TTNY distribution and identification of a reliable reaction model arise because of the fact that it is very difficult to obtain such data from experimental measurements involving various combinations of targets and projectiles at different projectile energies. In this paper we make an attempt to find out a suitable nuclear reaction model code for estimation of TTNY. In Sec. II, we describe the experimental procedure and data unfolding technique. In Sec. III, we discuss the procedure adopted to calculate thick target neutron yield distributions and the different models that we have used for our calculations. We compare our experimental and theoretical results and discuss them in Sec. IV.

II. EXPERIMENTAL PROCEDURE

Accelerated alpha particles in the energy range 30–50 MeV from the cyclotron at the Variable Energy Cyclotron Centre, Kolkata, have been directed on thick targets of ^{46}Ti and ^{27}Al. The beam energy resolution is about 200 keV for 30–50 MeV incident α's. The projectile energies, and the target thickness used are shown in Table I. The targets, 25 mm in diameter have been fixed perpendicular to the beam axis. The thickness of the targets are such that the incident alphas are completely stopped in the target while the scattering and absorption of neutrons produced in the target are negligible.

The neutrons emitted at 0°, 30°, and 45° with respect to incident beam direction are measured with a 52.4 mm ϕ

TABLE I. List of targets, projectile energies, and target thickness.

Target	Energy(MeV)	Thickness (mm)
^{46}TI	30,40,50	4.0 ± 0.05
^{27}Al	30,40,50	3.5 ± 0.05

$\times$52.4 mm NE-213 liquid scintillator kept at a distance of 1.4 m from the target. The detector angle of acceptance is 2.14° and energy resolution is about 20%.

A collimator at a distance of 20 cm in front of the target is used to restrict the beam size to about 10 mm. The beam current is minimized on the collimator and maximized on the target. The beam falling on the collimator has always been kept below 15% of the beam on the target, thus reducing the background neutron contribution to a negligible proportion. The target is surrounded by a suppressor grid (-100V). Beam currents used for the experiment are of the order of 100 nA. The maximum uncertainty in the measured beam current is estimated to be about 5%. The energy calibration of the system is done by ^{137}Cs (0.66 MeV) and ^{22}Na (0.51 and 1.2 MeV) γ rays using the method outlined in Ref. [8].

In order to estimate background contribution from room-scattered neutrons, a shadow bar is interposed between the detector and the target. The perspex shadowbar of length 100 cm and diameter 10 cm stops the direct contribution of neutrons produced from the target. The neutron spectrum measured with the interposed shadow bar gives the contribution of room-scattered neutrons which is finally subtracted from the original spectrum to obtain the corrected neutron emission spectrum.

The pulse height output distributions are unfolded to obtain neutron energy spectra with the revised FERDO unfolding code using the Monte Carlo calculated response functions [9]. The total error associated with unfolded spectra consists of (i) the statistical error associated with the measurement, (ii) the error arising from discretization of the continuous spectra and of the response function, and (iii) the statistical error inherent in the Monte Carlo calculation.

III. THEORETICAL MODEL CALCULATION

A. Thick target neutron yield distribution

When a projectile is incident on a thick target, it interacts with the target nuclei present at different depths in the target with continuously degrading energies. The observed emitted spectrum is a sum of emissions due to all these projectile energies within the target. We divide the target into a number of thin slabs, calculate the neutron emission spectra from each slab, and sum them to obtain the total emitted spectrum. The thickness of each slab is so selected that the projectile loses ΔE MeV energy in each slab. The kinetic energy of the projectile incident on the ith slab E_α^i and the average energy, $\overline{E_\alpha^i}$ in the ith slab are given by

$$E_\alpha^i = E_\alpha^0 - (i-1)\Delta E, \tag{1}$$

$$\overline{E_\alpha^i} = (E_\alpha^i + E_\alpha^{i-1})/2. \tag{2}$$

The slab thickness x_i is

$$x_i = \int_{E_\alpha^i}^{E_\alpha^{i+1}} \frac{dE}{-dE/dx}, \tag{3}$$

where (dE/dx) is the α stopping power for the target material as taken from Ref. [10].

The neutron yield $\phi(\epsilon,\theta)$ at energy ϵ and direction θ is given by

$$\phi(\epsilon,\theta)d\epsilon d\theta = \sum_{i=1}^{m} \sigma(\overline{E_\alpha^i},\epsilon,\theta)d\epsilon d\theta N x_i \times \exp\left\{-N\left[\sum_{k=1}^{i-1}\sigma_{\rm abs}(\overline{E_\alpha^k})x_k\right]\right\}, \tag{4}$$

where N is the number of target atom per unit volume, $m = (E_\alpha^0 - E_\alpha^{\rm th})/\Delta E$, $E_\alpha^{\rm th}$ being the projectile threshold energy for neutron production. For $i=1$, the value of the exponential attenuation factor in Eq. (4) is taken to be unity. Here, $\sigma_{\rm abs}$ is the absoption cross section of the projectile in the target. We denote $\sigma(E_\alpha,\epsilon,\theta)$ as the emission cross section of neutrons of energy ϵ at an angle θ with respect to the projectile direction when a projectile of energy E_α is incident on a target nucleus. These cross sections are obtained using the three nuclear reaction model codes as mentioned earlier.

B. Differential neutron emission cross section

The present experimental data are analyzed in terms of the preequilibrium (PEQ) and equlibrium (EQ) models of neutron emission since for the projectile energies considered in our experiments only these two types of reactions are expected to play significant roles.

The double differential (energy-angle) neutron emission cross-section for a projectile incident on a target nucleus with an energy E_α can be obtained as

$$\sigma(E_\alpha,\epsilon,\theta)d\epsilon d\theta = \sigma_{\rm PEQ}(E_\alpha,\epsilon,\theta)d\epsilon d\theta + \sigma_{\rm EQ}(E_\alpha,\epsilon,\theta)d\epsilon d\theta, \tag{5}$$

where $\sigma_{\rm PEQ}(E_\alpha,\epsilon,\theta)$ and $\sigma_{\rm EQ}(E_\alpha,\epsilon,\theta)$ are, respectively, the cross sections of PEQ and EQ neutron emissions in the direction θ with energy ϵ. In order to estimate PEQ emissions, we have used three different nuclear reaction codes : (a) the extended exciton model formalism (PRECO-D2), which takes into account the emission of neutrons through the single-step direct, multistep direct, multistep compound, and compound nuclear evaporation process, (b) the fully preequilibrium approach (PEQAG), based on the master equations (usually several tens of coupled equations) of the model, which includes multiple particle and/or multiple gamma emissions, (c) the hybrid model code (ALICE-91) [3] where cluster emissions are included in the EQ component, calculated using the Weisskopf-Ewing formalism. We now briefly describe the formalism used in the different codes that we have used.

C. PRECO-D2

In this code relaxation of the target plus projectile composite nucleus is described in terms of multistep direct (MSD) and multistep compound (MSC) processes. It is assumed that as relaxation proceeds through the creation and annihilation of particle-hole (excitons) pairs in the MSD, there is at least one unbound particle in each stage. Such particles may be emitted any time. These emissions are of high energy and are predominantly in the forward direction. But in the MSC process, at each stage of the relaxation, all the particles remain bound (below the particle emission threshold). Emission from the bound excited particles can occur through statistical fluctuations in energy when sufficient energy is concentrated on a particle. These are relatively lower energy emissions and are symmetric about 90° center of mass (c.m.) angle. Relaxation of the composite nucleus proceeds either through MSD or through MSC process. In the exciton model, the target-projectile composite nucleus is assumed to reach compound nuclear equilibrium through a cascade of two body interactions. Each stage of the binary cascade is characterized by the number of excited particles (p) and holes (h). The sum $p+h$ is referred to as the exciton number and is denoted as n.

The total energy differential preequilibrium cross section $\sigma_{\mathrm{PEQ}}(E_\alpha,\epsilon)$ is the sum of the MSD and MSC components.

$$\sigma_{\mathrm{PEQ}}(E_\alpha,\epsilon)=\sigma_{\mathrm{MSD}}(E_\alpha,\epsilon)+\sigma_{\mathrm{MSC}}(E_\alpha,\epsilon), \tag{6}$$

where E_α and ϵ are projectile and ejectile energies, respectively. Kalbach [11] evaluates the MSD component from the relation

$$\sigma_{\mathrm{MSD}}(E_\alpha,\epsilon)=\sigma_{\mathrm{abs}}\sum_{p=p_0}^{\bar{p}} S_d(p,h)T_u(p,h)\lambda_b^u(p,h,\epsilon), \tag{7}$$

where p_0 is the number of particles excited at the first stage of binary cascade and $\bar{p}$ is the number of excited particles in the equilibrated compound nucleus. The summation over p ensures contributions from all stages of the cascade. Here $S_d(p,h)$ is the probability of the formation of the (p,h) configuration with at least one unbound particle from earlier configurations which all had at least one particle in continuum. $T_u(p,h)$ is the mean lifetime of the (p,h) configuration and $\lambda_b^u(p,h,\epsilon)$ is the emission rate of the b-type particle with energy ϵ from the (p,h) configuration. Kalbach [12] calculates $S_d(p,h)$ and $T_u(p,h)$ by separately evaluating the phase-space available to the bound and unbound excited particles in each (p,h) configuration.

The total preequilibrum cross section $\sigma_{\mathrm{PEQ}}(E_\alpha,\epsilon)$ is evaluated using the standard Griffin exciton model and the MSC component is obtained as

$$\sigma_{\mathrm{MSC}}(E_\alpha,\epsilon)=\sigma_{\mathrm{PEQ}}(E_\alpha,\epsilon)-\sigma_{\mathrm{MSD}}(E_\alpha,\epsilon). \tag{8}$$

Also, included in the Kalbach formalism are two classes of direct reactions which are not taken into account in the calculation of MSD component from Eq. (7). These are nucleon transfer and nucleon knock-out reactions. These are evaluated semiempirically.

The neutron angular distributions are evaluated from the Kalbach-Mann (KM) systematics [11] where the preequilibrium angular distribution is broken up into two components — the MSD and the MSC. Nucleon transfer (σ_N) and nucleon knock-out (σ_{KO}) are included in the MSD while the evaporation component σ_{evap} is included in MSC. For a given projectile energy E_α, the double differential cross section is

$$\sigma(E_\alpha,\epsilon,\theta)=a_0(MSD)\sum_{l=0}^{l_{\max}} b_l P_l(\cos\theta) + a_0(\mathrm{MSC})\sum_{l=0}^{l_{\max}} b_l P_l(\cos\theta),$$

$$a_0(\mathrm{MSD})=\frac{1}{4\pi}[\sigma_{\mathrm{MSD}}(E_\alpha,\epsilon)+\sigma_N(E_\alpha,\epsilon)+\sigma_{KO}(E_\alpha,\epsilon)], \tag{9}$$

$$a_0(\mathrm{MSC})=\frac{1}{4\pi}[\sigma_{\mathrm{MSC}}(E_\alpha,\epsilon)+\sigma_{\mathrm{evap}}(E_\alpha,\epsilon)].$$

The coefficients b_l are functions of the ejectile energy and are assumed to be of the form

$$b_l=\frac{2l+1}{1+\exp[A_l(B_l-\epsilon-\beta)]}. \tag{10}$$

Here, β is the separation energy of the ejectile from the composite system. The parameters A_l and B_l are free parameters and have been obtained in the KM systematics by fitting with observed angular distribution as

$$A_l=[0.036+0.0039l(l+1)]\ \ \mathrm{MeV}^{-1},$$

$$B_l=\left\{98-\frac{90}{[l(l+1)]^{1/2}}\right\}\ \ \mathrm{MeV}^{-1}. \tag{11}$$

D. PEQAG

In the master equation form of the exciton model the preequilibrium decay is governed by a set of master equations. In order to be able to handle properly cascade of γ quanta in the model, the set of master equations of the exciton model was enlarged so as to couple different excitation energies (E) and various nuclei (i) [1,13]. The model estimates γ emission within the same formalism up to the total deexcitation of a nucleus, independently of a possible particle emission prior to or between the successive γs. The corresponding enlarged set of master equations reads

$$-D_{n,E,i}=\tau(n-2,E,i)\lambda^+(n-2,E,i)+\tau(n+2,E,i)\lambda^-(n+2,E,i)-\tau(n,E,i)[\lambda^+(n,E,i)+\lambda^-(n,E,i)+L(n,E,i)] + \sum_{j,m,x}\int_\epsilon \tau(m,E',j)\lambda_x^c(m,E',j,\epsilon)d\epsilon, \tag{12}$$

where $D_{n,E,i}$ is the initial exciton configuration of the composite system (taken to be $p=A_p$, $h=0$, where A_p is the projectile mass number, and $1p1h$ for the reactions induced by γ's). Here, $(\lambda^{\pm})$'s are the transition rates (per unit time) to the neighbor states, τ is the lifetime of the configuration and L is the total emission rate (including particles and γ's), integrated over the outgoing energy and summed over all possible emission channels of the specified exciton states,

$$L(n,E,i)=\sum_x \int_\epsilon \tau(n,E,i)\lambda_x^c(n,E,i,\epsilon)d\epsilon, \tag{13}$$

where λ_x^c is the emission rate of x-type nucleons.

The last term in Eq. (13) ensures the coupling of different nuclei and various excitation energies. The transition as well as the emission rates depend on the densities of n-exciton states in a given nucleus (the composite and the residual one). These densities are usually approximated using the equidistant-spacing scheme, what leads to the Ericsson type formulas. Explicit treatment of the Pauli principle (two excitons cannot share the same level) results in nonanalytical expressions, which can be well reproduced by Williams' formula [14]

$$\rho_{n=p+h}(E)=\frac{g(gE-A_{ph})^{p+h-1}}{p!h!(p+h-1)!}, \tag{14}$$

where we have put separately the particle (p) and the hole (h) numbers (total exciton number, $n=p+h$). A_{ph} stands for the Pauli correction to the partial level density and is defined as

$$A_{ph}=\frac{p^2+p+h^2-3h}{4g}. \tag{15}$$

For higher energies, the densities are modified as to take into account the finite depth of the nuclear potential well [16]. The transition rates are [15,17]

$$\lambda^+(n,E)\cong\frac{2\pi}{\hbar}|M|^2\frac{g(gE-A_{ph})^2}{2(n+1)},$$

$$\lambda^-(n,E)\cong\frac{2\pi}{\hbar}|M|^2\frac{g}{2}ph(n-2), \tag{16}$$

Here the appearance of an extra factor of 2 in the denominator is due to the indistinguishability of particles or holes. The nucleon emission rates are in their standard form [18].

$$\lambda_x^c(n,E,\epsilon)d\epsilon_x=\frac{2s_x+1}{\pi^2\hbar^3}\mu_x\epsilon_x\sigma_{\rm inv}(\epsilon_x)\frac{\rho_{n-1}(U)}{\rho_n(E)}R_x(n)d\epsilon_x, \tag{17}$$

where s_x is the intrinsic spin of the ejectile, $\hbar$ is reduced Planck's constant, μ_x its reduced mass, $\sigma_{\rm inv}(\epsilon_x)$ is the inverse cross section of ejectile with energy ϵ_x being absorbed by the residual nucleus, $R_x(n)$ is the effective factor, which simulates the two-component nature of the problem (for any

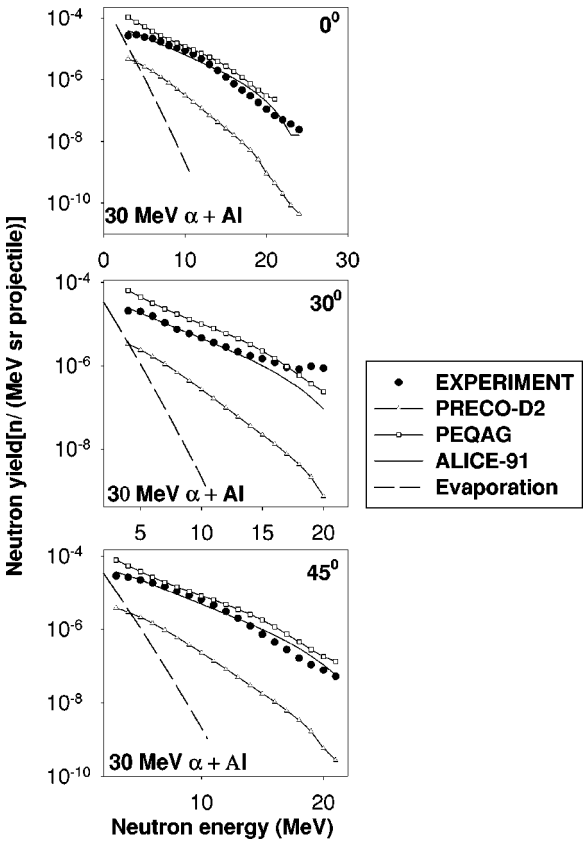

FIG. 1. Neutron yield distributions at 0°, 30°, and 45° for 30 MeV α particles bombarding thick Al targets. Measured data (solid circles) are compared with calculated results from PRECO-D2, PEQAG, and ALICE91 codes. Dashed lines are evaporation components calculated using ALICE91. Error bars in the experimental data are shown when they exceed the symbol size.

n-exciton state $R_p+R_n=1$). The transition matrix element $|M|^2$ is taken in its exciton number dependent form [19].

Finally, the energy-differential emission cross section is obtained as

$$\sigma(E_\alpha,\epsilon)=\sigma_{\rm abs}\sum_i\sum_n\int_E\tau(n,E,i)\lambda_x^c(n,E,i,\epsilon)dE. \tag{18}$$

The code PEQAG does not calculate angular distribution of emitted particles. We have obtained the double differential neutron emission cross section by using the KM systematics as

$$\sigma(E_\alpha,\epsilon,\theta)=\frac{1}{4\pi}\sigma(E_\alpha,\epsilon)\sum_{l=0}^{l_{\rm max}}b_lP_l(\cos\theta). \tag{19}$$

The assumption implicit in the above is that all emissions are from MSD-like processes. We have modified the code PEQAG to incorporate the above formulation.

E. ALICE91

The code ALICE-91 calculates PEQ emission of nucleons using the hybrid model followed by EQ emission of protons,

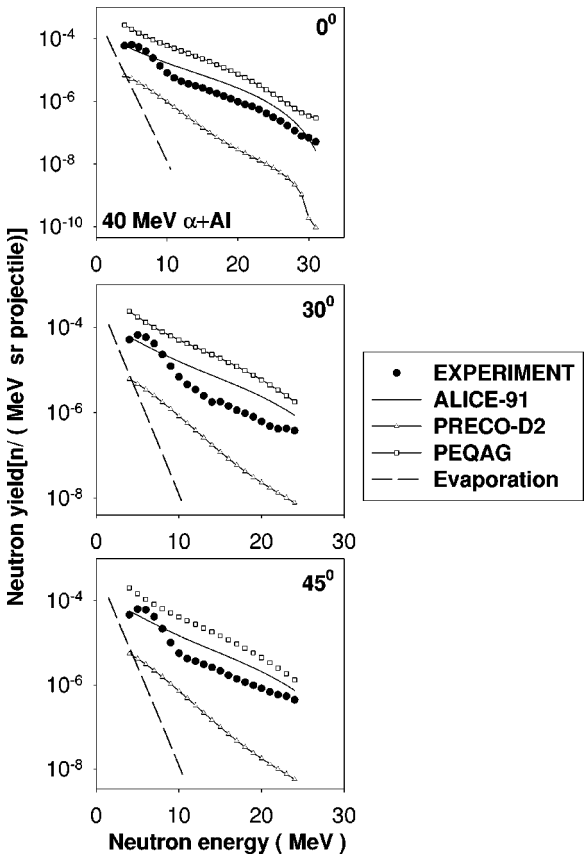

FIG. 2. Same as Fig. 1 for 40 MeV incident α energy.

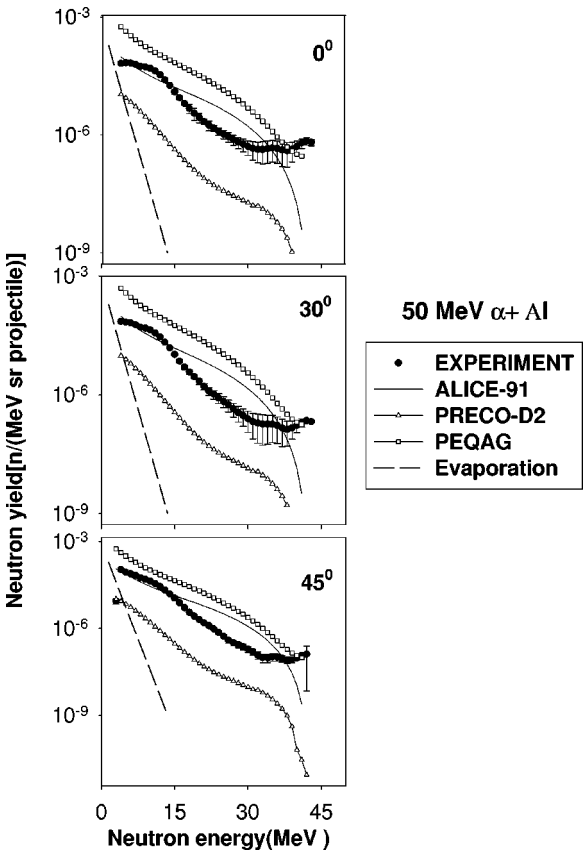

FIG. 3. Same as Fig. 1 for 50 MeV incident α energy.

neutrons, alpha-particles and deuterons using the Weisskopf-Ewing formalism. It considers PEQ emission of single neutron, single proton and simultaneously of two nucleons ($p-p$, $p-n$, $n-n$). PEQ emission of any cluster is not included.

In its mode of following the relaxation process, the hybrid model [20] combines the Boltzmann master equation and the exciton model. Each stage of the relaxation process is characterized by the exciton number (n) as in the closed form of the exciton model, i.e., using the ''never-come-back'' approximation, i.e., each two body interaction is assumed to increase n to $(n+2)$. However, instead of assuming an equal *a priori* probability for all energy distributions, the hybrid model explicitly evaluates the preemission energy distribution of the ejectile of interest in terms of appropriate intermediate (partial) state densities at each stage of the relaxation process. The hybrid model calculates the PEQ energy spectra of nucleon from the closed form expression [20–22]

$$\sigma_{\mathrm{PEQ}}(\epsilon_x)=\sigma_{\mathrm{abs}}\sum_{n=n_{0,\Delta n=2}}^{\bar{n}} D_n\left[{}_nX_x\frac{\rho_n(U,\epsilon_x)}{\rho_n(E_c)}\right]\frac{\lambda_c(\epsilon_x)}{\lambda_c(\epsilon_x)+\lambda_t(\epsilon_x)}, \tag{20}$$

where D_n is the depletion factor of nth exciton state (i.e., the probability of reaching the exciton state n without prior emission) and ${}_nX_x$ is the number of x type excited nucleons in it. Here $\rho_n(E_c)$ is the partial level density of the n exciton state at excitation energy E_c and $\rho_n(U,\epsilon_x)$ is the partial level density of the same n exciton state with the same energy E_c being distributed among n excitons in such a way that one particle-exciton have the energy ϵ_x+B_x and the rest $(n-1)$ excitons share the energy $U=E_c-\epsilon_x-B_x$, B_x being the separation energy of x. The ratio $\rho_n(U,\epsilon_x)/\rho_n(E_c)$ gives the probability of finding one x-type nucleon in the n-exciton state with energy ϵ_x+B_x prior to emission. The factor in the square bracket thus gives the number of x-type nucleons with energy ϵ_x+B_x in the n-exciton state. The last factor in Eq. (20) is the emission probability of x with energy ϵ_x and $\lambda_c(\epsilon_x)$ is the emission rate given by [22]

$$\lambda_c(\epsilon_x)=\frac{(2s_x+1)\mu_x\epsilon_x\sigma_{inv}(\epsilon_x)}{\pi^2\hbar^3 g}, \tag{21}$$

where g is the single particle level density of the composite nucleus and other symbols are as defined for Eq. (17). The total two body interaction rate $\lambda_t(\epsilon_x)$ that competes with the emission rate $\lambda_c(\epsilon_x)$ is given by the empirical relation

$$\lambda_t(\epsilon_x)=[1.4\times10^{21}(\epsilon_x+B_x)-6.0\times10^{18}(\epsilon_x+B_x)]/K. \tag{22}$$

Here K is an adjustable parameter. For $K=1$, the value of $\lambda_t(\epsilon_x)$ is equal to the interaction rate obtained from dividing nucleon velocity by the nucleon mean free path (MFP) inside the nucleus. Empirical values of $K>1$ are used in order to account for Pauli blocking which effectively increases the mfp inside the nuclear matter.

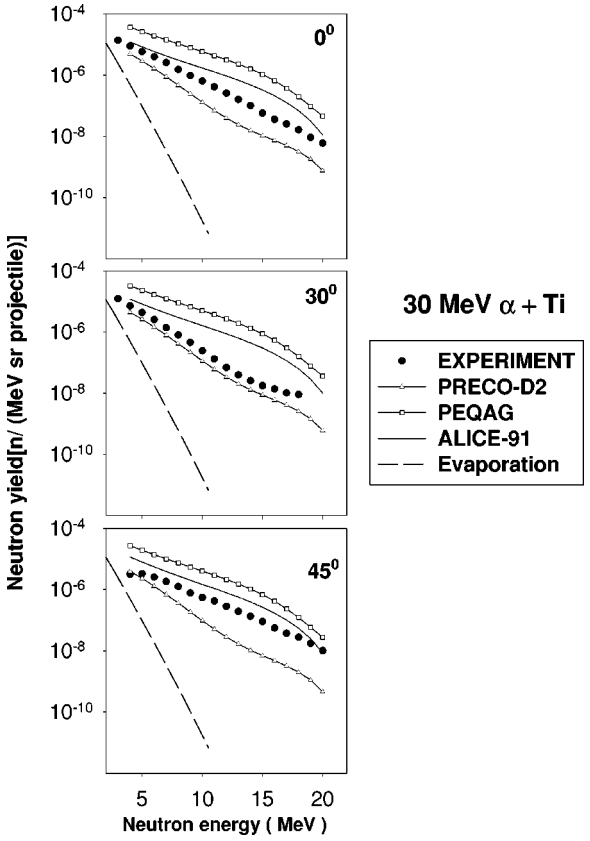

FIG. 4. Neutron yield distributions at 0°, 30°, and 45° for 30 MeV α particles bombarding thick Ti targets. Measured data (solid circles) are compared with calculated results from PRECO-D2, PEQAG, and ALICE91 codes. Dashed lines are evaporation components calculated using ALICE91. Error bars in the experimental data are shown when they exceed the symbol size.

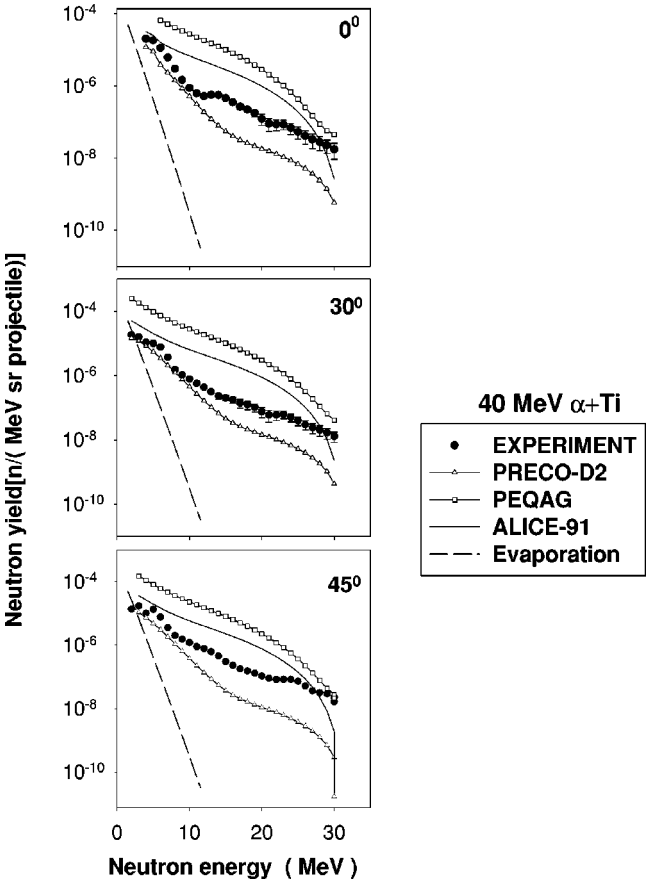

FIG. 5. Same as Fig. 4 for 40 MeV incident α energy.

The hybrid model evaluates the PEQ spectrum under the ''never-come-back approximation,'' i.e., each two-body interaction is assumed to always increase n to $n+2$ by creating a particle-hole pair. The effect of annihilating a particle-hole pair is completely neglected in Eqs. (20) and (21). This assumption is reasonably valid at the early stages of the nuclear relaxation process when the creation rate of a particle hole pair is dominating over the annihilation rate but is certainly questionable at later stages when this dominance no longer exists.

IV. COMPARISON OF MEASUREMENT WITH THEORETICAL CALCULATIONS

Neutron emission spectra from thick targets measured experimentally at different laboratory angles are plotted in Figs. 1–9, along with those calculated using the codes ALICE91, PRECOD2, and PEQAG. The evaporation contributions calculated using ALICE91 are also shown in the figures as dashed lines. Figures 1–3 show the spectra for $\alpha+$Al and Figs. 4–6 show the spectra for $\alpha+$Ti at 0°, 30°, and 45° emission angles for the projectile energies 30, 40, and 50 MeV, respectively. Figures 7–9 show the neutron emission spectra for 30 MeV proton induced reactions on Cu, Fe, and Pb at emission angles of 0°, 30°, and 45°. The experimental data for these proton induced reactions are from Ref. [4].

Default input options have been used for all the codes. An initial exciton configuration of $4p0h$ (four particles, zero holes) has been used for all calculations involving α induced reactions. For proton induced reactions the initial configuration of $2p1h$ (two particles, one hole) has been adopted. To calculate emission rates, inverse cross sections $\sigma_{\rm inv}$ have been calculated using the algorithm of Chatterjee *et al.* [23] in PEQAG and PRECOD2, while in ALICE91 the classical sharp cut off algorithm has been used. For calculation of absorption cross section $\sigma_{\rm abs}$, ALICE91 uses parabolic model routine for α projectiles and optical model algorithm for protons, while PEQAG and PRECOD2 use the algorithm by Chatterjee *et al.* In ALICE91 and PRECOD2, Fermi gas level density parameters are used in the Weisskopf-Ewing formalism to calculate emissions through the evaporation process. On the other hand PEQAG does not have a separate evaporation algorithm, the master equation calculations are continued even after the system reaches equilibrium. For PEQ emissions, PRECOD2 considers emission of only a single nucleon, while ALICE91 considers single and simultaneous two nucleon PEQ emissions. However, ALICE91 does not take into account successive multiple PEQ emissions as is done in PEQAG. Another important difference among the codes is the energy distribution of the nucleus in the composite system prior to emission in the PEQ phase. PRECOD2 using the closed form exciton model does not explicitly calculate preemission en-

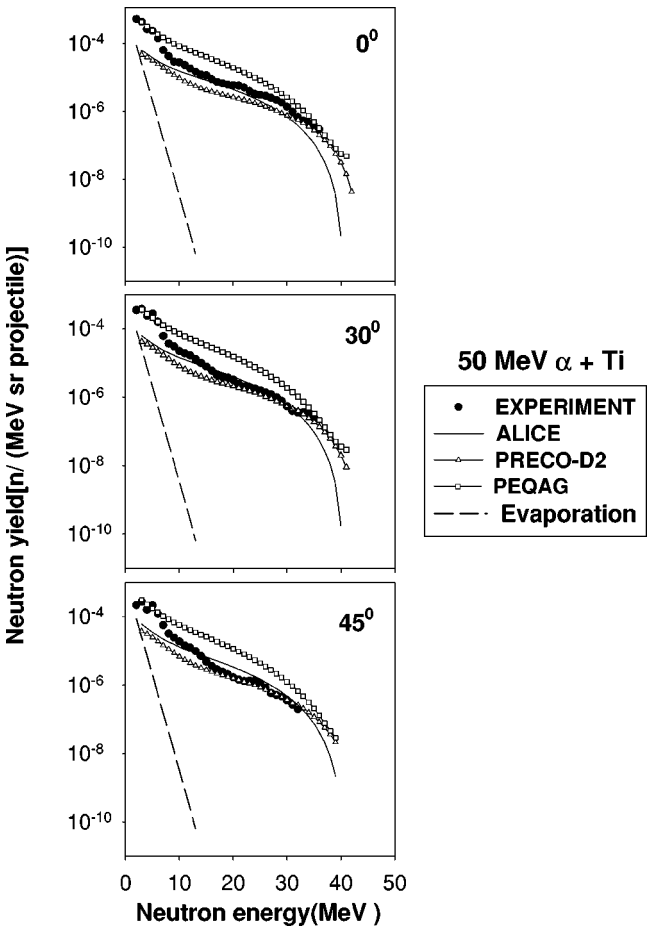

FIG. 6. Same as Fig. 4 for 50 MeV incident α energy.

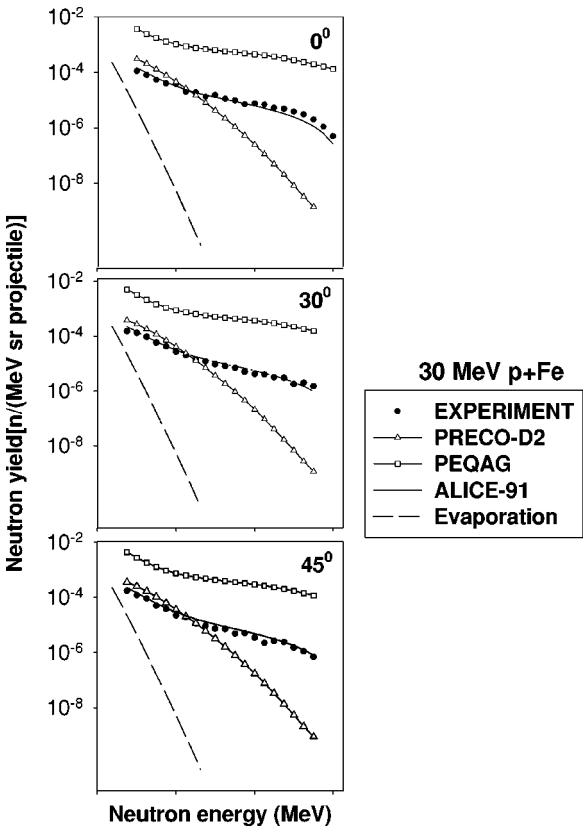

FIG. 7. Neutron yield distributions at 0°, 30°, and 45° for 30 MeV protons bombarding thick Cu targets. Measured data (solid circles) are compared with calculated results from PRECO-D2, PEQAG, and ALICE91 codes. Dashed lines are evaporation components calculated using ALICE91. Error bars in the experimental data are shown when they exceed the symbol size.

ergy distribution of the excited particles, but considers that all energy distribution are equally probable. On the other hand, ALICE91 and PEQAG calculate the energy distribution based on the density of states.

It is seen that for 30 MeV α on Al (Fig. 1) ALICE91 reproduces the measured neutron spectra closely while PEQAG gives a slight overprediction and PRECO-D2 underpredicts the sprectra at all angles. For 40 MeV α on Al (Fig. 2) both ALICE91 and PEQAG overpredict the spectra though ALICE91 gives closer approximation to the measured distribution. PRECO-D2 underpredicts the spectra. For 50 MeV incident α energy (Fig. 3), ALICE91 overpredicts the neutron emission spectra in the energy range 15 to 40 MeV. PEQAG gives some overprediction and PRECO-D2 continues to underpredict the measured data.

For the reaction $\alpha+{}^{46}$Ti, it is seen that for 30 and 40 MeV incident α energies (Figs. 4 and 5), ALICE91 overpredicts the neutron spectra at all angles for high emission energies. But at 50 MeV incident energy (Fig. 6), the observed angular distribution is well reproduced by the hybrid model, though for neutron emission energies greater than about 37 MeV there is a slight underprediction. Results from PEQAG overpredict the measured distribution slightly more than that for the Al target. Calculated results using PRECO-D2 underpredict the measured spectra for 30 and 40 MeV incident energies, but for 50 MeV, the observed distribution is fairly well reproduced. At 40 MeV incident energy the low energy part of the emitted neutron spectra is consistent with PRECO-D2 calculations.

Figures 7, 8, and 9 give the energy differential neutron yield distributions for 30 MeV proton induced reactions on Fe, Cu, and Pb at 0°, 30°, and 45° of neutron emission angles. The experimental data is from Ref. [4]. Calculations have been done with all aforementioned three codes. It is observed here that ALICE91 calculations reproduce the experimental data very closely whereas PEQAG overestimates and PRECO-D2 grossly underestimates the observed data. In this case the PRECO-D2 calculations underestimate the high energy component of the estimated neutron distribution to a larger extent.

The general observation from the above comparison is that ALICE91 reproduces experimental measurements more closely than the other two codes. PEQAG gives a consistant overprediction while PRECO-D2 underestimates the measured data.

ALICE91 calculates the nucleon-nucleon interaction rate using the empirical relation (22). Though the calculated values from Eq. (22) were compared against those obtained from optical model potential [22], the empirical nature may be the cause of some overprediction of the calculated spectra at 50 MeV α energy. Underprediction of the high energy

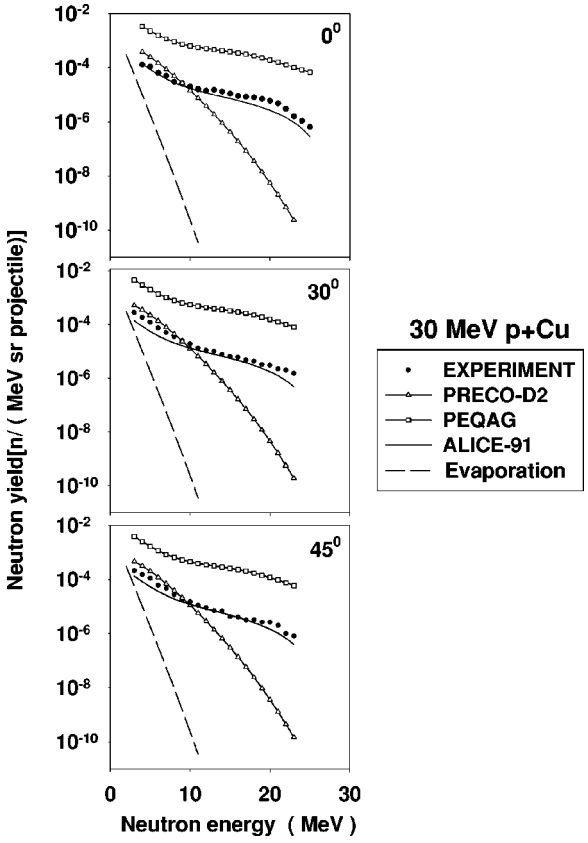

FIG. 8. Neutron yield distributions at 0°, 30°, and 45° for 30 MeV protons bombarding thick Fe targets. Measured data (solid circles) are compared with calculated results from PRECO-D2, PEQAG, and ALICE91 codes. Dashed lines are evaporation components calculated using ALICE91. Error bars in the experimental data are shown when they exceed the symbol size.

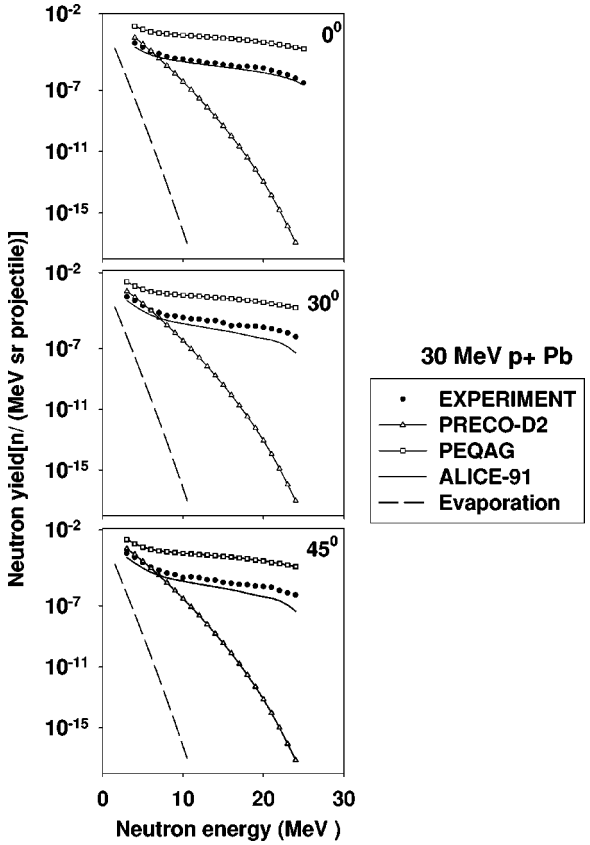

FIG. 9. Neutron yield distributions at 0°, 30°, and 45° for 30 MeV protons bombarding thick Pb targets. Measured data (solid circles) are compared with calculated results from PRECO-D2, PEQAG, and ALICE91 codes. Dashed lines are evaporation components calculated using ALICE91. Error bars in the experimental data are shown when they exceed the symbol size.

component of the emitted neutron spectra particularly at high incident enegies may be due to the absence of direct reaction calculations in ALICE91. Contribution from the direct reactions become significant at high projectile as well as ejectile energies.

PRECO-D2 calculates the total PEQ cross section using the closed form exciton model. The original exciton model of Griffin does not explicitly calculate the preemission energy distribution of the excited particles, but considers that all energy distributions are equally probable. As a result, the high energy part of the PEQ emission probability is underpredicted. Moreover, PRECO-D2 considers only single nucleon PEQ emission. The underprediction of the measured spectra may be attributed to these factors. Although the Kalbach formalism takes into account two types of direct reactions, namely, nucleon transfer and nucleon knock-out, these processes may not be important at lower projectile energies. Particularly the contribution from the nucleon transfer mechanism is small for low projctile and target mass numbers. Such underpredictions of PRECO-D2 calculations have been discussed in details in Ref. [7].

The exciton model code PEQAG uses the extended ''master equation'' approach to calculate the PEQ neutron emission from the reactions studied. The neutron distributions calculated with PEQAG mostly overpredict the measured values for 40 and 50 MeV α energies. For 30 MeV incident α particle, the high energy part of emitted neutron spectra are slightly underpredicted. In the extended master equation, the probability of occupying a particular energy state at a given exciton number is considered. Secondly, in the formalism used, PEQ emission of particles from several intermediate nuclei is considered. These may have removed the underprediction caused by the original exciton model to some extent.

Our study showed that there exist some mismatch between the reaction cross sections of the projectile used in the three codes. But this difference is not sufficient to remove the discrepancy between the neutron distribution calculated by them. When the spectra are normalized for this difference, even then the angular distributions calculated by ALICE91, PRECO-D2, and PEQAG differ by a large extent. In order to calculate the two-body collision rate ALICE91 uses an empirical formula [22] by Blann (22). But the exciton model estimates two body interaction rates using the matrix element $|M|$ in Eq. (16). This might have resulted in different values of the emission probability calculated by ALICE91 and PEQAG.

There may be two reasons for the overpredictions observed in PEQAG calculations. First of all, the absorption cross section σ_{abs} is higher in the case of PEQAG compared to

ALICE91. However, the σ_{abs} calculated in PEQAG is only about 20% higher than that of ALICE91 and this does not account for the large overpredictions in some of the cases.

The other possible source is in the evaluation of the factor $R_x(n)$ in PEQAG and ${}_nX_x$ in ALICE91. These two factors determine the number of neutrons or protons constituting the n excitons. In ALICE91, after the initial exciton configuration (which is an input parameter for all the codes) the next configuration is determined from the relative number of neutrons and protons in the composite system as well as the relative strengths of neutron-proton (dissimilar nucleons) and neutron-neutron or proton-proton (similar nucleons) interactions. It considers that the interaction strength of dissimilar nucleons are three times larger than that for similar nucleons. For higher exciton configurations ALICE91 populates those states by exciting equal number of neutrons and protons irrespective of their relative abundance in the composite system. In PEQAG, on the other hand, all the higher exciton states after the initial are populated by neutrons with probability N/A and by protons with probability Z/A, where N and Z are the numbers of neutrons and protons, respectively, and $A=N+Z$, in the composite system. For a composite system with relatively large number of neutrons, the exciton population will have larger neutron fraction. This eventually leads to higher neutron emission resulting in large overpredictions in the case of Ti ($N/A=0.52$), Fe($N/A=0.54$), Cu($N/A=0.54$), and in Pb($N/A=0.6$) for calculations with PEQAG.

V. CONCLUSIONS

We have experimentally measured neutron yield distributions from thick targets of Al and Ti bombarded by α particles of 30, 40, and 50 MeV. The measurements have been carried out at laboratory angles of 0°, 30°, and 45°. The experimental data are compared with the calculated results from three different codes, namely, PEQAG, PRECO-D2, and ALICE91 based on the exciton model or its variant. Modifications in the codes have been made to calculate thick target neutron yield distributions from the double differential neutron yield cross sections. Comparisons have been done also with measured data of others for 30 MeV proton induced reactions. It is observed that the code ALICE91 gives the overall best agreement with the experimental data. PRECO-D2 underestimates the measured distributions significantly. PEQAG calculations show slight to moderate and large overestimations when compared with the experimental observations. Such comparisons provide useful information about the codes that are required to be used for calculating neutron yield data, which are gaining importance presently.

[1] E. Betak and J. Dobes, Report No. IP EPRC SAS 43/(1983), Bratislava, 1983.
[2] C. Kalbach, Report No. LA-10248-MS, Los Alamos National Laboratory, Los Alamos, 1985.
[3] M. Blann, Lawrence Livermore National Laboratory Report No. UCID 19614, 1982; International Centre for Theoretical Physics Workshop on Applied Nuclear Theory and Nuclear Model Calculations for Nuclear Technology applications, Trieste, Italy, SMR/284-1, 1988.
[4] K. Shin, K. Hibi, M. Fujii, Y. Uwamino, and T. Nakamura, Phys. Rev. C **29**, 1307 (1984).
[5] K. Shin, Y. Uwamino, and T. Hyodo, Nucl. Technol. **53**, 78 (1981).
[6] T. Nakamura and Y. Uwamino, Phys. Rev. C **29**, 1317 (1984).
[7] P.K. Sarkar, T. Bandopadhyay, G. Muthukrishnan, and S. Ghosh, Phys. Rev. C **43**, 1855 (1991).
[8] G. Dietze, IEEE Trans. Nucl. Sci. **NS-26**, 398 (1979).
[9] Y. Uwamino, K. Shin, M. Fujii, and T. Nakamura, Nucl. Instrum. Methods **204**, 179 (1982).
[10] C.F. Williamson, J.P. Boujot, and J. Picard, Centre Etudes Nucleari res de Saclay Report No. CEA-R 3042, 1966.
[11] C. Kalbach and F. M. Mann, Phys. Rev. C **23**, 112 (1981); C. Kalbach, *ibid.* **25**, 3197 (1982).
[12] C. Kalbach, Phys. Rev. C **23**, 124 (1981); **24**, 819 (1981).
[13] E. Betak, Ric. Sic. Educ. Perm., Suppl. 66 p. 92, University of Milano, 1988 (unpublished).
[14] F. C. Williams, Jr., Nucl. Phys. **A166**, 231 (1971).
[15] F.C. Williams, Jr., Phys. Lett. **31B**, 184 (1970).
[16] E. Betak and J. Dobes, Z. Phys. A **279**, 319 (1976).
[17] P. Oblozinsky, I. Ribansky, and E. Betak, Nucl. Phys. **A226**, 347 (1974).
[18] C.K. Cline, Nucl. Phys. **A193**, 417 (1972).
[19] C. Kalbach, Z. Phys. A **287**, 319 (1978).
[20] M. Blann, Phys. Rev. Lett. **27**, 337 (1971); **27**, 700 (E) (1971); **27**, 1550 (E) (1971).
[21] M. Blann, Nucl. Phys. **A213**, 570 (1973).
[22] M. Blann and H.K. Vonach, Phys. Rev. C **28**, 1475 (1983).
[23] A. Chatterjee, K.H.N. Murthy, and S.K. Gupta, Pramana **16**, 391 (1981).